Journal of Catalysis **198,** 56–65 (2001)
doi:10.1006/jcat.2000.3071, available online at http://www.idealibrary.com on IDEAL®

The State of Cu Promoter Atoms in High-Temperature Shift Catalysts—An *in Situ* Fluorescence XAFS Study

Peter Kappen, Jan-Dierk Grunwaldt,*[,1] Birgitte S. Hammershøi,* Larc Tröger, and Bjerne S. Clausen*

*Hamburger Synchrotronstrahlungslabor HASYLAB at Deutsches Elektroneu-Synchrotron DESY, Notkestrasse 85, D-22603 Hamburg, Germany; and *Haldor Topsøe A/S, Nymøllevej 55, DK-2800 Lyngby, Denmark*

Received June 26, 2000; revised September 4, 2000; accepted September 14, 2000; published online February 8, 2001

The state of the copper promoter (0.17–1.5 wt%) was studied in Fe–Cr-based high-temperature shift (HTS) catalysts by *in situ* fluorescence XAFS combined with on-line gas analysis. The XANES spectra acquired in the fluorescence mode showed that Cu is present as copper metal under working conditions of the high temperature shift catalyst but easily reoxidizes upon air exposure at room temperature. In contrast, the active chromium substituted magnetite phase is stable under these conditions as shown by X-ray diffraction (XRD). Both as-prepared and used (i.e., after HTS run) catalysts were studied during reduction in 2%H_2/3%H_2O/N_2. For the used catalyst, an intermediate Cu(I) phase is detected by *in situ* fluorescence XANES. The reduction of Cu(II) to Cu(I) occurred at 120–150°C, nearly independent of the Cu concentration, whereas the stability of the Cu(I) phase toward further reduction was significantly dependent on the Cu concentration, being especially high at low copper concentration. For the as-prepared HTS catalysts the initial reduction started at around 250°C, during which Fe(III) and Cr(III)/Cr(VI) containing phases were transformed to a chromium substituted magnetite phase. The copper reduction occurred simultaneously with the reduction of the iron matrix. Thus, the reduction temperature of Cu(II) was significantly shifted to lower temperatures for catalysts which were previously reduced in the HTS reaction. It is proposed that Cu(II) is incorporated into iron and chromium containing phases in the as-prepared catalysts and segregates out forming small metallic clusters on the surface of the oxide phases during activation/reaction. © 2001 Academic Press

1. INTRODUCTION

The water gas shift reaction (WGSR), in which carbon monoxide reacts with steam to yield carbon dioxide and hydrogen according to the following scheme,

$$CO + H_2O \rightleftarrows CO_2 + H_2 \quad \Delta H = -40.6 \text{ kJ/mol},$$

is used industrially for both hydrogen production and ammonia synthesis (cf. 1, 2). Since the reaction is exothermic and reversible, the water gas shift reaction is, for thermodynamic and kinetic reasons, normally performed in two steps. In the first step a high-temperature shift (HTS) catalyst, usually based on Fe_2O_3/Cr_2O_3, is used for equilibration of the WGSR at 340–530°C. The second step is normally performed on a low temperature shift (LTS) catalyst, based on $CuO/ZnO/Al_2O_3$ at 180–230°C.

Typically, HTS catalysts comprise 88–92% Fe_2O_3 and 8–12 wt% Cr_2O_3 (1). Additionally, different promoters, e.g., copper, lead, cobalt, magnesium, and zinc can be used (1, 3–6). Several studies have been performed to investigate the kinetics of the conversion of CO (see, e.g., 1, 2), and to study the role of the iron oxide and chromium oxide phases (1, 7–9). From XRD, TPR, and Mössbauer studies (1, 3, 7, 9, 10) it is well-known that the Fe(III) phases (e.g., α-FeO(OH), α-Fe_2O_3, γ-Fe_2O_3) are reduced and transformed to the magnetite phase, Fe_3O_4, upon activation in the reaction mixture of the WGSR, and chromium is incorporated into the magnetite phase in oxidation state +3. The magnetite phase, where the cations are placed in tetrahedral A sites and octahedral B sites with a unit cell written as $(Fe_8^{3+})_A$ $(Fe_8^{3+}\ Fe_8^{2+})_B O_{32}$ ("inverse spinel structure," cf. (11)), is the active component in the HTS catalysts (1, 3, 7). Pure Fe_3O_4 is not thermoresistent enough at the temperatures applied in the HTS reaction and will deactivate due to sintering. Cr_2O_3 is therefore supposed to act as textual promoter, by retarding sintering and consequently loss of surface area (1, 7–9). Cr enters the magnetite lattice presumably as Cr^{3+} on the B sites (12). Koy *et al.* (8) recently performed molecular modeling calculations on the substitution of iron by chromium and also found that Cr fits well into the hematite and magnetite lattice and forms a superstructure in the iron oxide lattice.

Much less is known on the role of other promoters in HTS catalysts. Copper promoted Fe–Cr catalysts are, e.g., reported to exhibit higher activity and selectivity, especially at low steam to CO ratios, where the formation of methane and other aliphatic hydrocarbons is favored (1, 4, 6). Structural studies are rare, which is probably due to the fact that the concentration of the promoter atoms is too low to allow the application of most characterisation techniques.

[1] To whom correspondence should be addressed. Fax: (+45) 45 27 29 99. E-mail: jdg@topsoe.dk.

0021-9517/01 $35.00
Copyright © 2001 by Academic Press
All rights of reproduction in any form reserved.

The development of techniques, which can provide structural information under *in situ* conditions, is strongly desired in catalyst research. Both transmission X-ray absorption fine structure (XAFS) and X-ray diffraction (XRD) give the possibility of performing structural characterization when the catalyst is in its working environment (13). However, the application of these techniques is typically restricted to systems with relative high concentrations of the element of interest. The study of elements with low concentrations is often the case in heterogeneous catalysis, especially when the role of promoters or of poisons is subject to studies. Moreover, in noble metal catalysts (e.g., Pt, Ir, Rh, Au), the metal concentration is often low due to the high cost of the noble metal and due to the high dispersion achieved at low concentrations. For such catalyst systems a method with enhanced sensitivity needs to be applied.

In this respect fluorescence XAFS may be a useful technique (14–16), but the efficiency of the detectors used has been too low to allow dynamic *in situ* studies. However, with the recent progress in X-ray fluorescence detection and the development of multielement silicon drift detectors (SDDs) with integrated junction field effect transistor (JFET) (17–21), much higher count rates (a few 100,000 cts/s) with low noise level (peak to background ratio (P/B) $\approx 10^3$) and good energy resolution (<350 eV) can be obtained (19, 20, 22). With such detectors XAFS studies become possible on very diluted samples (below 100 ppm) (20, 22), and *in situ* scans of low concentrated systems become achievable on a reasonably short timescale (22). Moreover, the SDDs can be operated at room temperature and thus do not need the attachment of bulky cryogenic cooling equipment as other solid state detectors (23), e.g., germanium detectors. The potential of SDDs in comparison to commercially available multielement germanium detectors lies in the very high count rate capability (several hundred thousand counts per second per pixel at energy resolutions <350 eV). Furthermore, silicon technology in principle allows complete integration of detector chip and front-end electronics in multielement design. Both aspects are important to minimize data collection time for time-resolved studies. While we use a seven-element detector in this study, a 61-element SDD module is currently under development (24). Finally, it can be combined with a glass capillary microreactor cell, as previously used in *in situ* transmission XAFS and XRD measurements (13, 25–27). This makes the application of the fluorescence XAFS technique interesting not only for diluted liquid systems and thin films but also in the field of catalysis.

We will show here the application of this combination of a reaction cell with on-line gas analysis and the *in situ* fluorescence technique with a seven-element SDD to the investigation of the copper promoter phase in the high-temperature water gas shift catalysts. For this purpose, several Cu promoted Fe–Cr-based catalysts were studied with respect to the oxidation state of copper before and after catalytic tests. Moreover, the reduction mechanism of Cu was studied for catalysts with different loadings and catalysts subjected to different pretreatments. The advantage of this novel *in situ* fluorescence XAFS method is also discussed in view of transmission XAFS results on the same catalysts.

2. EXPERIMENTAL

A. In Situ Fluorescence and Transmission XAFS Experiments

The *in situ* transmission and fluorescence XAFS experiments were performed at the bending magnet beamline X1 at HASYLAB at DESY (Hamburg, Germany). A Si(111) double-crystal monochromator was used for controlling the photon energy at the sample. The beam intensity was monitored by an ionization chamber and stabilized via a monochromator feedback system. By detuning the crystals to 50% of the maximum intensity higher harmonics were effectively rejected. The setup of the *in situ* fluorescence XAFS technique will be described in more detail in another publication (22). It consisted of a seven-element SDD and of an *in situ* cell, which was previously also used for *in situ* transmission EXAFS/XRD experiments (13, 25–27). The SDD was operated at room temperature and placed perpendicular to the beam in order to minimize the detection of elastic scattering from the sample (16). The capillary tube was positioned such that the synchrotron beam hit the sample in a 30° angle in order to illuminate as much as possible of the sample and to be able to move the SSD close to the sample (around 5 cm, resulting in a solid angle per pixel of ca. $4\pi \times 0.02\%$). The silicon drift detector was additionally protected with aluminium foil and cooled by an air fan to prevent heating from the reaction cell.

The signals of the SDD detector (silicon chip by KETEK, Munich, each of the 7 pixels having an active area of 5 mm^2) were amplified and recorded as described in Ref. (22). Typically about 70,000 cts/s were obtained from a flat sample disk but due to the smaller monochromator exit slit and the larger distance to the sample only about 35,000–40,000 cts/s were obtained from the samples loaded in the capillary cell. Fluorescence XAFS scans were acquired around the Cu *K*-edge (8980 eV). Under static catalyst conditions good quality spectra were recorded between 8800 and 9660 eV with acquisition times up to 60 min (5 s acquisition time/point with smaller steps around the edge). Additionally, faster scans (8–10 min) were taken during reduction (8950–9100 eV, 5 s acquisition time/point). The whole system was controlled by the beamline software ON-LINE (28). The data from each of the seven elements were corrected for the dead time of the detection system, normalized to an

edge jump of 1 and then added up by using weighting factors estimated from the statistical quality of the data (22).

As *in situ* reaction cell for the combined XAFS and temperature-programmed reduction experiments, a quartz capillary (outer diameter 1.5 mm; wall thickness 0.01 mm) plug flow reactor, filled with about 50 mg catalyst, was used. For this purpose the catalyst pellets were crushed and a sieve fraction of 75–125 μm was used. From a flow system different premixed gases were fed through the capillary cell. The outlet gas was analyzed with a mass spectrometer (Balzers Thermostar). Enclosing the reactor in an X-ray transparent heat shield ensured temperature homogeneity. Further details of the capillary reactor system can be found in Ref. (25). The temperature-programmed reduction was performed *in situ* by using 2% H_2/N_2 saturated with H_2O at room temperature (giving about 3 vol%) and a continuous heating ramp of 1.5 K/min.

In the case of transmission EXAFS the incident and transmitted X-ray intensities were recorded by the use of N_2-filled ionization chambers. Spectra of Yb_2O_3 were recorded simultaneously in order to have an internal energy calibration. XAFS spectra were recorded between 8700 and 9660 eV by step scanning the monochromator. Cu-foil, CuO, and Cu_2O were used as model compounds.

B. Samples

Four different copper promoted catalysts were investigated and are listed in Table 1. All catalysts contained Fe : Cr in a molar ratio 10 : 1 and were derived from commercially available Fe–Cr catalysts.

The catalysts A and B had been used under water gas shift conditions prior to characterization. Catalyst A contained 1 wt% Cu and has been in operation at 400–420°C, 24 atm for 1000 h at HTS conditions. The dry feed contained about 18% CO, 12% CO_2, 70% H_2 and steam was added to give a steam-to-dry gas ratio of 0.7. The catalysts were cooled down in nitrogen, exposed to air, and thereafter used for more detailed characterization. In order to understand the influence of the copper concentration on the activity, sample B was prepared by extraction of copper from sample A with several portions of 6 M aqueous ammonia solution, washed with water and finally dried at 100°C. Interestingly, the copper could not be removed to a lower extent than 0.17 wt%. Generally, copper promoted samples were found to exhibit higher activity than the unpromoted ones, as also reported in Refs. (1, 4, 6). However, catalyst A and B showed the same HTS activity, although the copper concentration was different.

TABLE 1

Overview on the Catalyst Used for *in Situ* Fluorescence EXAFS

Catalyst	Molar ratio Fe : Cr	Cu in wt%	Pretreatment	Phase analysis by XRD
A	10 : 1	1.0	After catalytic test	Magnetite phase ($a_0 = 8.380$ Å)
B	10 : 1	0.17	After catalytic test	Magnetite phase ($a_0 = 8.372$ Å)
C	10 : 1	1.0	As-prepared and calcined	α-Fe_2O_3, γ-Fe_2O_3, some FeOOH
D	10 : 1	1.5	As-prepared and calcined	α-Fe_2O_3, γ-Fe_2O_3, some FeOOH

Catalysts C and D were obtained by impregnation of a standard Fe–Cr-based catalyst with 0.43 and 0.65 M Cu nitrate solutions, respectively. After impregnation the tablets were dried at 100°C and then calcined at 350°C for 2 h in order to decompose the Cu nitrate.

The samples were first investigated *ex situ*. Then all catalysts were reduced at temperatures up to 480°C in 2% H_2/3% H_2O/N_2 at a total flow of about 5 Nml/min. (Gas flow in units of Normmilliliter (Nml), i. e., related to standard conditions of 0°C and 101.3 kPa.)

3. RESULTS

3.1. Characterization of the Copper Promoted Catalysts

According to XRD (Table 1) and Mössbauer studies on similar catalysts (not shown), the main phase of the two catalysts, which have been under reaction conditions (catalysts A and B), is a chromium substituted magnetite ($Fe_{3-x}Cr_xO_4$). Therefore the lattice parameter a_0 is slightly lower (catalyst A, $a_0 = 8.372$ Å; catalyst B, 8.380 Å) compared to 8.395 Å in case of pure magnetite (29, 30). No copper phases could be detected by X-ray diffraction.

Scanning electron microprobe analysis, performed on the catalyst pellet with low Cu concentration (after extraction of copper), revealed that Cu was homogeneously distributed on the sample. As an example the distributions of Fe, Cr, and Cu of sample B are shown in Fig. 1. The distribution of Fe, Cr, and Cu is very similar across the whole catalyst pellet, also at the outer part of the pellet. This shows that the deposition and the extraction of copper led to a catalyst pellet, where copper has been extracted homogeneously from the whole pellet.

The calcined and fresh catalyst samples C and D contained mainly hematite (α-Fe_2O_3) and maghemite (γ-Fe_2O_3) accompanied by some FeOOH (Table 1). No Cr- and Cu-containing phases were found by XRD. Chemical analysis showed that the samples C and D contained about 1.28 wt% Cr(VI) and 1.35 wt% Cr(VI), respectively. Electron microprobe analysis of these samples revealed that the Cu concentration was homogeneous through the whole catalyst pellet.

3.2. Ex Situ Fluorescence XAFS Investigation of the Used Catalysts

Figure 2 depicts the multichannel analyzer fluorescence spectra (MCA) of samples A and B, obtained at an

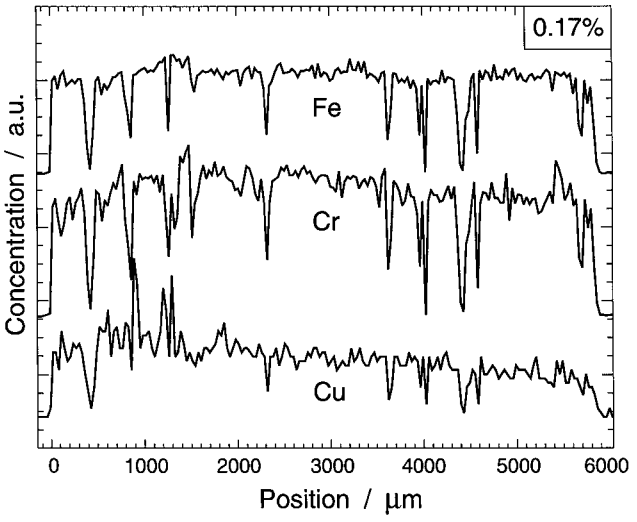

FIG. 1. Scanning micro probe (beam size 20 μm) analysis of Fe, Cr, and Cu across a catalyst pellet (diameter 5.9 mm) of catalyst B, the spikes originate from the sample preparation process for the microprobe analysis (i.e., a thin plate is cut).

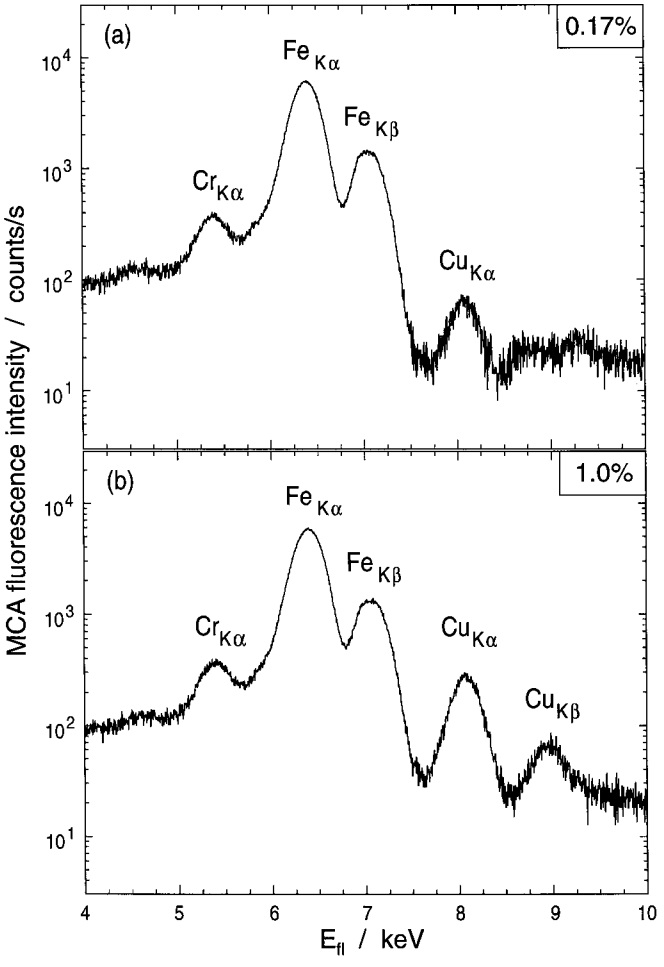

FIG. 2. Multichannel analyzer energy spectra of Cu promoted Fe–Cr-based HTS catalysts ($E_{\text{excit.}} = 12{,}700$ eV) with (a) 0.17 wt% Cu loading (catalyst B) and with (b) 1.0 wt% Cu loading (catalysts A).

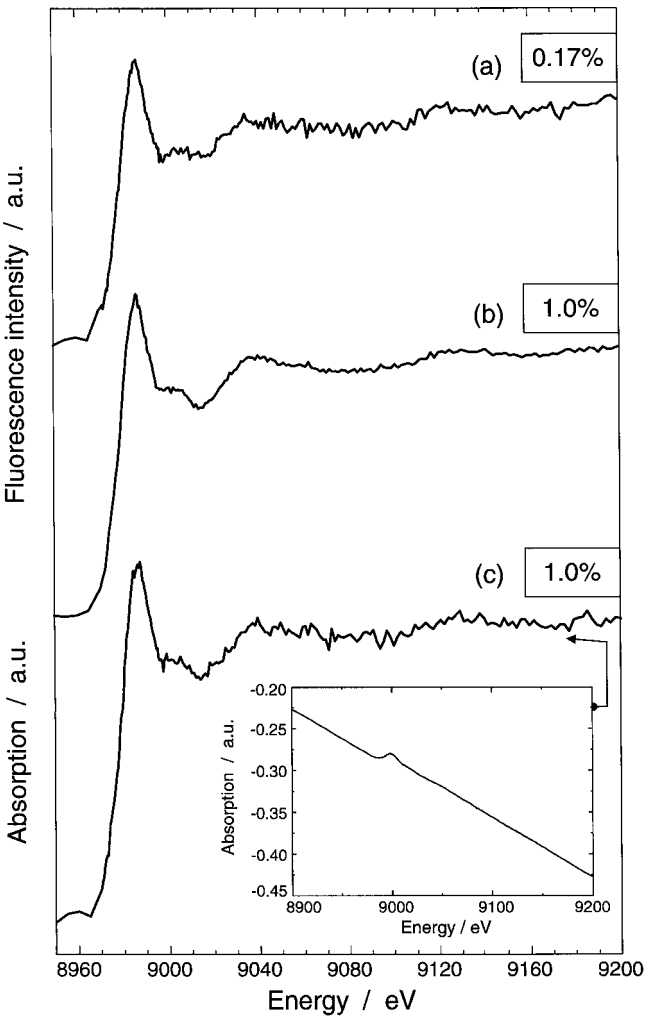

FIG. 3. Fluorescence and transmission XAFS spectra around the Cu *K*-edge of CU-promoted HTS catalysts at room temperature: (a) fluorescence XAFS spectra of sample with 0.17 wt% Cu loading (measured in the capillary, catalyst B); (b) fluorescence XAFS spectra of sample with 1.0 wt% Cu loading (measured as pellet, catalyst A); (c) transmission EXAFS of sample with 1.0 wt% Cu (measured as pellet, catalyst A, after background subtraction); Inset shows transmission EXAFS data of catalyst A without background subtraction.

excitation energy of 12,700 eV. Traces a and b in Fig. 3 show the corresponding fluorescence XAFS spectra around the Cu *K*-edge of catalysts B and A. The fluorescence lines of CuK_α at 8040 eV in Figs. 2a and 2b are well separated in both cases from the other fluorescence lines of CrK_α at 5400 eV, FeK_α at 6400 eV, and FeK_β at 7060 eV (cf. for the tabulated positions of the florescence lines; e.g., Ref. 31). In case of the 1.0 wt% promoted sample, additionally, the CuK_β line at 8910 eV is observable and the intensity of the CuK_α line is significantly higher than for the 0.17 wt% promoted sample. The net copper fluorescence count rate of sample B was about 1/6 that of sample A, nicely reflecting the different Cu loadings.

The XAFS spectra of the two catalysts (Fig. 3a and b) are quite similar, both exhibiting a strong white line. The edge energy for catalyst A was found to be at 8986 eV and for catalyst B at 8988 eV. Above the edge only weak oscillations are present. For comparison the 1.0 wt% Cu promoted catalyst was also measured with transmission XAFS (Fig. 3c and inset). The sample was carefully prepared in such a way that optimum conditions were obtained for transmission EXAFS (pellet with absorption length $\mu \cdot d = 1.5$) and the spectrum was collected for 60 min to obtain good statistics, a factor two longer than the fluorescence XAFS spectra of Fig. 3. As seen from the inset in Fig. 3 the edge jump is very small ($J = 0.01$), but after background subtraction (curve c in Fig. 3), the same spectral features as seen with fluorescence XAFS can be observed. However, the noise is significantly lower in the case of spectra obtained in the fluorescence mode (P/B ratio ca. 200). Sample B could not be measured with transmission EXAFS in a reasonable time frame due to the very low Cu concentration in the quite heavy matrix of Fe and Cr which absorbs a large fraction of the synchrotron radiation.

As mentioned above the XAFS measurements revealed a distinct white line in the spectra originating from Cu(II). Also the weak oscillations above the edge and the edge energies of 8986 eV (1 wt% Cu) and 8988 eV (0.17 wt% Cu), respectively, correspond to that of a Cu(II) species. There might be a slight shoulder in sample A (1 wt% Cu), but no shoulder in the Cu *K*-edge is found in case of sample B (0.17 wt% Cu), indicating that Cu(II) is placed on sites with centro-symmetric geometry. The small shoulder in the edge of sample A suggests that the geometry is slightly distorted (32–34).

3.3. *In Situ Investigation of Catalysts A and B during Reduction*

In order to investigate the oxidation state of Cu under reaction conditions and the stability of Cu(II)/Cu(I) species in the matrix, reduction of the catalysts was performed in the 2% H_2/3% H_2O/N_2 gas mixture which has a similar reduction potential as that of the industrial water gas shift reaction mixture (2, 9). Figures 4 and 5 show selected *in situ* near edge fluorescence XAFS spectra on catalysts B and A. They were recorded at selected temperatures during *in situ* reduction with the constant heating rate of 1.5 K/min. The insets show all fluorescence XAFS scans taken during the experiment. For both catalysts the starting spectrum is similar to that shown in Figs. 3a and 3b. Around 150°C the white line decreases (Figs. 4 and 5, trace b) and spectra with a distinct pre-edge appear. However, the splitting of the white line and stronger oscillations at higher energies, typical of the formation of metallic Cu (cf. (26), and Fig. 6), occurs only at higher temperatures (Fig. 4, trace e; Fig. 5, traces d and e). It is obvious from Figs. 4 and 5 that the full reduction to Cu(0) is terminated at lower temperatures

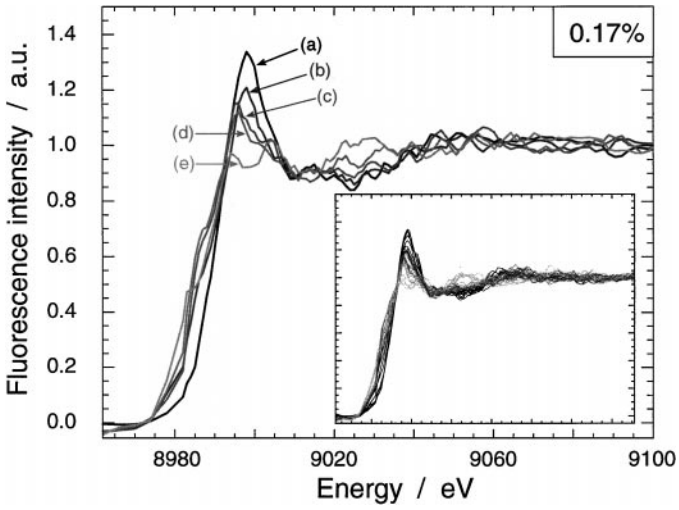

FIG. 4. Selected *in situ* fluorescence XANES scans during the reduction in 2% H_2/3% H_2O/N_2 at (a) 50°C, (b) 150°C, (c) 250°C, (d) 350°C, (e) 480°C at the Cu *K*-edge of the 0.17wt% Cu promoted HTS catalysts (catalyst B, sample time about 10 min); Inset shows all XANES spectra, downscaled 1 : 2.

for the catalyst with the higher copper loading (catalyst A). In the simultaneously recorded temperature programmed (TPR) spectra, no hydrogen consumption was observed. This is expected since the amount of hydrogen needed to reduce the very low amount of Cu is too low to be measured by the mass spectrometer (less than 10 μmol Cu compared to a flow of 0.2 mmol H_2/min).

Interestingly, the reduction of copper starts at about the same temperature for the catalysts A and B and it can be speculated that the reduction proceeds via a Cu(I)

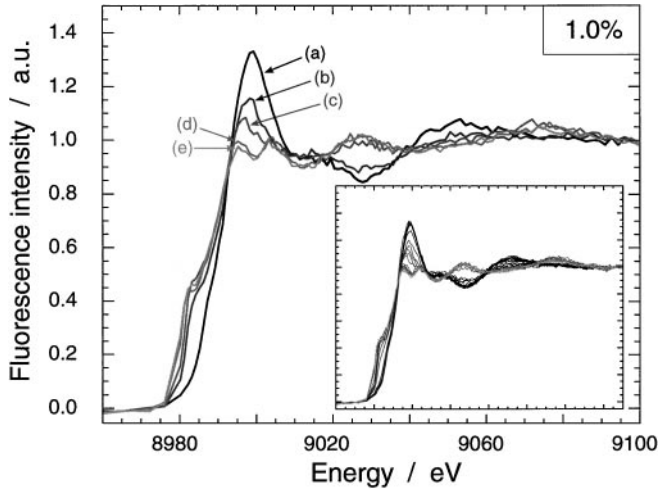

FIG. 5. Selected *in situ* fluorescence XANES scans during the reduction in 2% H_2/3% H_2O/N_2 at (a) 50°C, (b) 150°C, (c) 200°C, (d) 300°C, (e) 480°C at the Cu *K*-edge of the 1.0 wt% Cu promoted HTS catalysts (catalyst A, sample time about 10 min); Inset depicts all XANES spectra, downscaled 1 : 2.

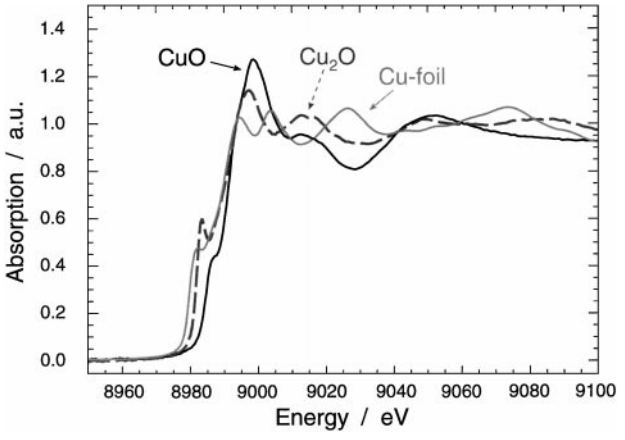

FIG. 6. Transmission XAFS at the Cu *K*-edge of model samples: Cu-foil, Cu_2O, CuO.

intermediate state. In order to quantify these observations it may be useful to study the near edge structure of copper with respect to Cu(II), Cu(I), and Cu(0), as one can see from the model samples, depicted in Fig. 6. The following spectral features may be used to interpret the different Cu oxidation states:

(a) intensity of the white line at a fixed energy (or the maximum value of the white line in a normalized spectrum);
(b) position of the edge (e.g., the first maximum of the first derivative of a normalized spectrum);
(c) intensity of the pre-edge (e.g., pre-edge height in a normalized spectrum at a fixed incident photon energy of 8985.50 eV).

The near edge structure of XAFS of the Cu *K*-edge has also previously been used to determine the oxidation state of copper (32, 33, 35–37). In Fig. 7 the position of the edge, determined from the first derivative of the normalized spectrum, and the intensity of the pre-edge as function of reduction temperature are depicted. The intensity of the white line decreases and shows therefore a similar trend. In case of catalyst B (Fig. 7a, 0.17 wt% Cu promoted sample) there is a change in edge energy of ca. 6 eV to lower values at about 120°C. This energy shift is slightly higher than the value of 4 eV observed from CuO to Cu_2O. The energy shifts again 2 eV further down at about 380°C. Similarly, the intensity of the pre-edge exhibits a maximum as one would expect in case of a Cu(I) intermediate (Fig. 6). The pre-edge band is due to the "1*s*–4p_z" atomic transition, which occurs when Cu(I) is in planar or linear geometry (32, 33, 37). However, the change is not as abruptly as in case of the edge energy shift. This can be interpreted as a mechanism where the valence state of Cu sharply changes, whereas the symmetry around the Cu atom only slowly changes to a linear or planar geometry with more intense 1*s*–4p_z transition. Also the white line decreases in two steps (Fig. 4, traces a to b, and d to e) due to the formation of the intermediate Cu(I) phase.

In case of catalyst A (Fig. 7b; 1.0 wt% Cu promoted sample) the first reduction step also proceeds at about 150°C, as concluded from the energy shift of the edge and the intensity change of the pre-edge, but complete reduction is already terminated at 220°C. From the position of the edge energy and the height of the white line (Fig. 5, traces b and c) one can conclude that a Cu(I) intermediate phase is formed, but it is stable in a significantly narrower temperature interval than for catalyst B. In contrast to catalyst B, the intensity of the pre-edge does not show a pronounced intermediate state for catalyst A. Hence, the existence of the intermediate Cu(I) phase is dependent on the Cu concentration.

Note that it was not possible by chemical extraction to remove more copper than down to 0.17 wt% from the matrix in this type of catalyst. The obviously enhanced stability of copper in catalyst B is discussed in more detail in Section 4. Copper might be more strongly bound to the matrix structure or the copper cluster formation is hindered at low concentrations. Catalyst A may also contain such more stable copper species which, however, is not observable because of the higher overall copper concentration.

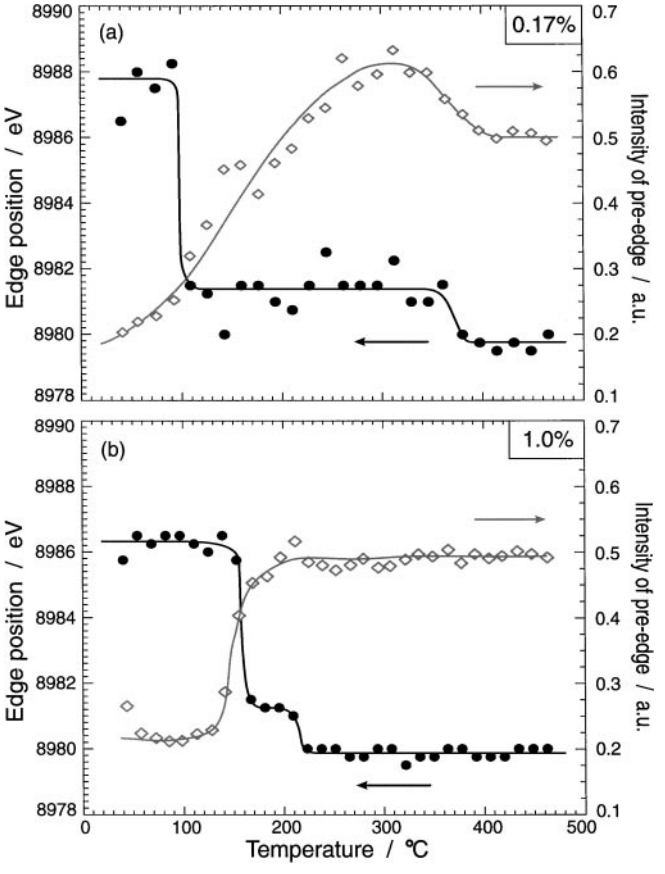

FIG. 7. Cu *K*-edge energies and the intensity of the Cu pre-edge as function of the reduction temperature in HTS catalysts; (a) 0.17 wt% promoted (catalyst B) and (b) 1.0 wt% Cu (catalyst A).

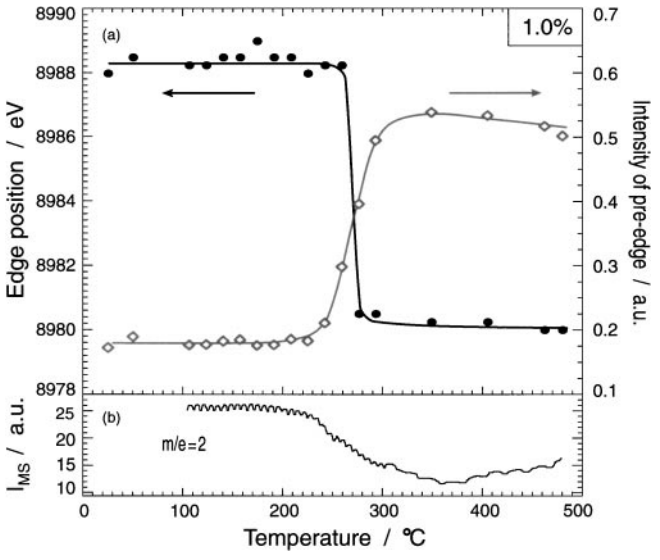

FIG. 8. *In situ* reduction of HTS catalyst with 1.0 wt% Cu (as-prepared Fe–Cr catalyst, catalyst C in Table 1): (a) Cu *K*-edge energies and the intensity of the Cu pre-edge extracted from the fluorescence XAFS spectra as function of the reduction temperature in HTS catalysts; (b) H_2 response in the MS (TPR spectrum).

3.4. In Situ Reduction of the as-Prepared Catalysts C and D

The TPR traces of the as-prepared copper catalysts C and D are given in Figs. 8b and 9b and the simultaneously recorded fluorescence XAFS spectra (analyzed in the same way as in Section 3.2) in the corresponding Figs. 8a and 9a.

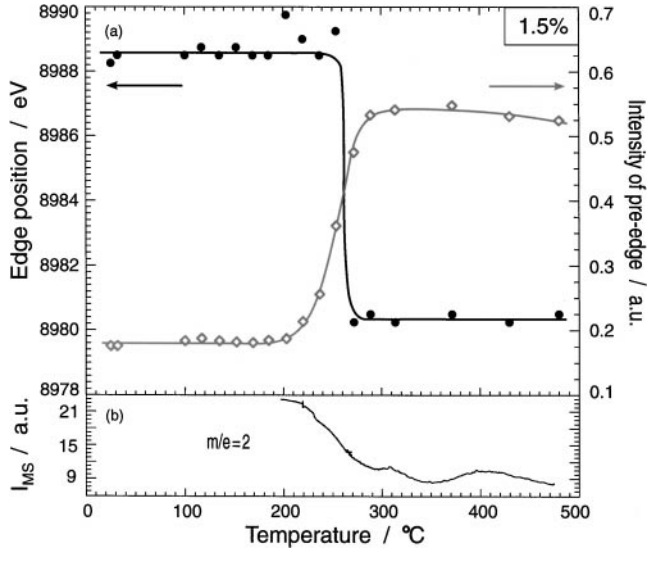

FIG. 9. *In situ* reduction of HTS catalyst with 1.5 wt% Cu (as-prepared Fe–Cr catalyst, catalyst D in Table 1): (a) Cu *K*-edge energies and the intensity of the Cu pre-edge extracted from the fluorescence XAFS spectra as function of the reduction temperature in HTS catalysts; (b) H_2 response in the MS (TPR spectrum).

Significant hydrogen consumption is found for both catalysts (Figs. 8b and 9b). In the case of the used catalysts (Section 3.2) no hydrogen consumption was observed because the Fe(III) phases were already reduced to Fe_3O_4 (and not reoxidized upon air exposure) and the consumption of hydrogen by copper was too low to be detected. Catalysts C and D in the as-prepared state comprise mainly Fe(III) and Cr(III)/Cr(VI) phases and therefore the hydrogen consumption is mainly due to reduction of 1/3 of the Fe(III) to Fe(II) and some Cr(VI) to Cr(III). In 50 mg of a catalyst about 1/3 of 0.56 mmol Fe can be reduced, which can be monitored by the mass spectrometer. From the analysis (Section 3.1) it is furthermore known that about 1.3 wt% is present as Cr(VI) corresponding to about 0.016 mmol Cr(VI), which is probably reduced to Cr(III). The reduction of the Fe/(Cr) phases in both catalysts started at about the same temperature (≈250°C).

The analysis of the fluorescence XAFS spectra at the Cu *K*-edge (Figs. 8a and 9a) revealed that the edge position was in both cases located at 8988 eV and that the reduction of Cu also occurred around 250°C, compared to 150°C for the used catalysts (Fig. 7). According to the shift of the Cu *K*-edge energy and the intensity increase of the pre-edge (Figs. 8a and 9a), there is no indication of a stable Cu(I) intermediate phase. The shift in the energy of the Cu *K*-edge is about 8 eV, which is similar to that observed for catalyst B and fits quite well with the reduction of Cu(II) to Cu(0). The slightly larger shift compared to the reduction of CuO to Cu (6 eV) is probably due to the fact that there is no shoulder in the edge present as, e.g., in catalyst A and other Cu(II) model samples with Cu in slightly distorted symmetry (32, 33). The intensity of the white line was found to decrease slowly with increasing temperature, which suggests that the copper slowly migrates out of the matrix.

4. DISCUSSION

The reduction of iron in as-prepared catalysts, as observed by on-line mass spectrometric analysis, is very similar to TPR profiles of pure Fe–Cr catalysts (9). The reduction of the catalysts is found to be shifted to lower temperatures in our studies (250°C compared to 350°C in Ref. (9)), which presumably is an effect of the heating rate (1.5°C/min instead of 6°C/min in Ref. (9)), the preparation procedure, and/or an effect of the presence of the copper promoter atoms. The study shows that the microreactor plug-flow reactor applied in this study can give *in situ* information on the reduction of the catalyst matrix containing mainly Fe(III).

By use of a silicon drift detector (SDD) the fluorescence XAFS technique applied during *in situ* studies (i.e., TPR, MS-analysis) allows an identification of the state of Cu promoter atoms down to at least 2000 ppm. Although Fe and Cr have fluorescence lines in the energy region 5400 to 7000 eV, the energy resolution of the detector is sufficient to

separate the CuK_α line to obtain good statistics for *in situ* fluorescence XAFS runs. With the transmission EXAFS technique, spectra at the Cu *K*-edge cannot be recorded at such low concentrations (Section 3.2), especially because of the quite strong attenuation of the X-rays by the matrix atoms Fe and Cr. Since recording time is typically shorter for *in situ* studies in order to follow dynamic phenomena, the application of transmission EXAFS is limited for low concentrated samples. Also on-line gas-analysis requires a relatively large amount of sample which is not a problem for XAFS acquired in fluorescence mode but is in the case of transmission XAFS due to the requirements of optimum sample thickness. This becomes especially interesting in case of catalytic studies combined with structural characterization with XAFS. Typically, optimum sample thickness means in case of transmission XAFS small amounts of catalyst rendering catalytic conversion to be measured. Thus, catalytic studies can be combined only in selected cases with transmission XAFS (e.g., Ref. (38)). Another advantage of fluorescence XAFS is that it is not necessary to utilize a very homogeneous sample as in transmission EXAFS. Instead of the silicon drift detector a Ge detector could have been used, but the SDD was found to be advantageous for the reasons described in Section 1.

Interestingly, the copper reduction occurred in the fresh catalysts C and D at the same temperature (i.e., 250°C), where also the iron (chromium) reduction started (Section 3.4). In the used catalysts A and B the reduction already started at 150°C and 120°C, respectively. Additionally, in case of low loadings (catalyst B), a stable Cu(I) phase up to 380°C was detected by fluorescence XAFS. This shows that the reduction behavior of copper is strongly dependent on the pretreatment of the catalyst (as-prepared or after use in the HTS reaction) and the concentration of copper (catalyst A vs catalyst B). An effect of the matrix structure on the reduction temperature was also found for Cu–Zn catalysts. Ternary Cu–Zn–Al methanol catalysts are more difficult to reduce than binary Cu–Zn catalysts (39). Also copper in $CuAl_2O_4$ and in $CuCr_2O_4$ spinels has been reported to be more difficult to reduce than CuO (40, 41).

In the as-prepared catalysts C and D it can be speculated that Cu(II) is incorporated into the matrix of the Fe–Cr catalysts, which is presumably not the case in the used (prereduced) catalyst A. Several Cu–Fe and Cu–Cr phases have been described in literature, e.g., $CuFe_2O_4$, $CuCr_2O_4$, and $CuFeO_2$ (42). The first two phases are spinel structures with Cu on tetrahedral A sites. Hence, the incorporation of Cu(II) in other Fe or Cr containing phases is likely and is also supported by the following observations. The reduction of copper and that of the Fe–Cr matrix seem to start at the same time. Moreover, it was concluded from the near edge structure of the Cu *K*-edge that Cu(II) is placed on centro symmetric sites with low distortion (no strong pre-edge visible). As mentioned before (Section 3.4), the Cu(II) edge position is virtually shifted to higher energies in catalysts B, C, and D because no pronounced pre-peak is present as known from Cu(II) in slightly distorted symmetry (32–34). Therefore the shift of the edge energy during reduction of catalysts B, C, and D amounts to 8 eV and is significantly higher than that for the transformation of CuO to Cu (6 eV, Fig. 6). Interestingly, it is also higher than that observed for the prereduced (used) catalyst A.

Under the working conditions of the catalyst the copper promoter atoms appear to be in the reduced state. Cu reoxidizes upon air exposure (results not shown in present paper), whereas the chromium substituted magnetite phase is stable in air at room temperature. These results are in agreement with previous investigations (1, 3, 8, 9). The chromium-substituted magnetite phase with 1/3 Fe^{2+} in the lattice was described in Mössbauer and XRD studies (1, 3, 7, 9, 10). Cu quickly reoxidizes at room temperature, as also observed in methanol catalysts (38), probably due to the small Cu particle size. The easier oxidation of small copper particles compared to bulk copper was studied by Fubini and Giamello (43) and the easy oxidation of small copper particles was also found in the case of dissociative adsorption of N_2O (44). Since the reduction of the used catalyst A is easier compared to catalysts C and D and the shift in energy amounts only to 6 eV, copper seems to be segregated out of the Fe–Cr matrix during reduction and forms small metallic clusters on the surface of the oxide phases. These copper particles are reoxidized upon air exposure and a second reduction process (catalyst A, during the *in situ* run) occurs at lower temperature compared to catalyst C and D, where copper is not on the surface but incorporated into the lattice.

In case of catalyst B, the reduction is significantly different and it was also observed that copper could not be removed from the catalyst by chemical extraction down to less than 0.17 wt%. The reduction of the catalyst proceeds via an intermediate Cu(I) phase. The Cu(I) phase is stable over a large temperature range (150–350°C) which is unusual for copper phases. XAFS studies of CuO on Al_2O_3, SiO_2, and zeolite supports have shown that stable Cu(I) phases are formed by evacuation at 500°C (32, 35, 36, 37, 45, 46). Also during the reduction of $CuCr_2O_4$ it was speculated that a Cu^I species is formed (40, 41). The reduction of CuO in hydrogen, however, proceeds quickly to Cu metal and no intermediate phase can be found (cf. (42) and references therein). QEXAFS measurements on Cu/ZnO catalysts (loading ca. 5 wt%) have, e.g., also shown that the reduction occurs in a very narrow temperature interval (26). Only when using piezo-QEXAFS with a sample time of 4.45 s/spectrum, indication for an intermediate Cu_2O phase was found in case of $Cu/ZnO/Al_2O_3$ catalysts (47). In the present study the concentration of copper was significantly lower and we have seen that the stability of Cu(I) is strongly dependent on the concentration of copper. In case of sample A (1.0 wt% Cu)

the Cu(I) intermediate state has a much more narrow temperature interval where it is stable. The enhanced stability in sample B (0.17 wt% Cu) could therefore be due to hindered copper crystal formation with copper being more strongly bound to the magnetite. It can be speculated that a small amount of copper can reversibly go into the magnetite surface, because the ionic radius of the Cu(II) cation is small enough. As mentioned before, several Cu–Fe and Cu–Cr phases, $CuFe_2O_4$, $CuFeO_4$, $CuCr_2O_4$, and $CuCrO_4$ (40–42, 48), have been described in the literature. This would also explain the incomplete extraction of Cu.

Moreover, we have seen by XANES analysis of sample B that the valence state sharply changes (Cu(II) to Cu(I)), whereas the pre-edge intensity is only slowly altered. These observations indicate a slower change in the symmetry of the ligands around the Cu atom from tetrahedral to linear/planar geometry. Kau *et al.* (33) studied several Cu(I) model complexes to reveal the relationship between the intensity of the $1s$–$4p_z$ transition in the XANES spectra and the symmetry of the coordination shell. According to their data the pre-edge reduces in intensity when the coordination structure around Cu(I) goes from linear/planar to tetrahedral because no splitting of the $1s$–$4p$ transition takes place in tetrahedral coordination. A variation of the XANES spectra has recently also been observed by Kumashiro *et al.* (37), where the feature at 8.983 eV reduced remarkably in intensity upon CO adsorption on Cu(I) in zeolites. This was explained with the change of the coordination structure from planar to tetrahedral.

Hence, at small copper concentrations (catalyst B), Cu(I) is not only stable over a large temperature range (150–350°C) but it also seems to undergo a slow change from tetrahedral to planar/linear coordination. This again indicates that copper in small concentrations is stabilized by the Fe–Cr matrix. Work is in progress to further specify the role of Cu in the differently promoted Fe–Cr-based high-temperature shift catalysts.

5. CONCLUSIONS

The present study has shown that the *in situ* fluorescence XAFS technique combined with a capillary reactor and online mass spectrometric analysis can provide unique information of the structural properties of promoters in catalysts under working conditions. Using the silicon drift detector spectra can be recorded in a sufficiently short time scale with appropriate statistics so that structural transformations can be detected *in situ* and in a time-resolved manner.

The investigation of the state of copper in high temperature shift catalyst has given particular insight into the structure of the copper promoter phase in Fe–Cr-based catalysts. It was found that the reduction behavior of copper in pre-reduced high temperature shift catalysts is strongly dependent on the copper concentration. At low copper concentrations, the reduction proceeds via a relatively stable intermediate Cu(I) phase. Also the pretreatment of the catalyst is found to influence the reduction behaviour. The fluorescence XAFS technique will in general be of interest for the study of catalysts, where the element of interest is present at low concentration, e.g., noble metal catalysts, promoters, and poisons.

ACKNOWLEDGMENTS

The authors thank HASYLAB for offering beamtime, E. Törnqvist for helpful discussions, and A. Kjersgaard, S. Rokni, and M. Herrmann for their assistance during the EXAFS measurements. Financial support from DANSYNC is gratefully acknowledged.

REFERENCES

1. Kochloefl, K., *in* "*Handbook of Heterogeneous Catalysis*" (G. Ertl, H. Knözinger, and J. Weitkamp, Eds.), Vol. 4, p. 1831. Wiley-VCH, New York, 1997.
2. Bohlbro, H., "An Investigation on the Kinetics of the Conversion of Carbon Monoxide with Water Vapour over Iron Oxide based Catalysts," 2nd ed. Copenhagen, 1969.
3. Topsøe, H., and Boudart, M., *J. Catal.* **31**, 346 (1973).
4. Andreev, A., Idakiev, V., Mihajlova, D., and Shopov, D., *Appl. Catal.* **22**, 385 (1986).
5. Schneider, M., Pohl, J., Kochloefl, K., and Bock, O., "Iron Oxide–Chromium Oxide Catalyst and Process for High Temperature Water–Gas Shift Reaction." U.S. patent 4598062, 1986.
6. Huang, D. C., and Braden, J. L., "High Temperature Shift Catalyst." European patent application 0 353 453, 1990.
7. Doppler, G., Trautwein, A. X., Ziethen, H. M., Ambach, E., Lehnert, R., Sprague, M. J., and Gonser, U., *Appl. Catal.* **40**, 119 (1988).
8. Koy, J., Ladebeck, J., and Hill, J.-R., *Stud. Surf. Sci. Catal.* **119**, 479 (1998).
9. Gonzalez, J. C., Gonzalez, M. G., Laborde, M. A., and Moreno, N., *Appl. Catal.* **20**, 3 (1986).
10. Rethwisch, D. J., Philips, J., Chen, Y., Hayden, T. F., and Dumesic, J. A., *J. Catal.* **91**, 167 (1985).
11. Greenwood, N. N., and Earnshaw, A., "Chemistry of the Elements." Pergamon Press, Oxford, 1984.
12. Smit, J., and Wijn, H. P. J., "Ferrites." Wiley, New York, 1959.
13. Clausen, B. S., Topsøe, H., and Frahm, R., *Adv. Catal.* **42**, 315 (1998).
14. Jaklevic, J., Kirby, J. A., Klein, M. P., Robertson, A. S., Brown, G. S., and Eisenberger, P., *Solid State Commun.* **23**, 679 (1977).
15. Lytle, F. W., Greegor, R. B., Sandstrom, D. R., Marques, E. C., Wong, J., Spiro, C. L., Huffman, G. P., and Huggins, F. E., *Nucl. Instrum. Methods. Phys. Res.* **226**, 542 (1984).
16. Iwasawa, Y., "X-Ray Absorption Fine Structure for Catalysts and Surfaces," Vol. 2. World Scientific, Singapore, 1996.
17. Strüder, L., and Soltau, H., *Radiat. Prot. Dosim.* **61**, 39 (1995).
18. Cramer, S. P., Tench, O., Yocum, M., and George, G. N., *Nucl. Instrum. Methods Phys. Res. A* **266**, 586 (1988).
19. Lechner, P., Eckbauer, S., Hartmann, R., Krisch, S., Hauff, D., Richter, R., Soltau, H., Strüder, L., Fiorini, C., Gatti, E., Longoni, A., and Sampietro, M., *Nucl. Instrum. Methods Phys. Res. A* **377**, 346 (1996).
20. Gauthier, C., Goulon, J., Moguiline, E., Rogalev, A., Lechner, P., Strüder, L., Fiorini, C., Longoni, A., Sampietro, M., Besch, H., Pfitzner, R., Schenk, H., Tafelmeier, U., Walenta, A., Misiakos, K., Kavadia, S., and Loukas, D., *Nucl. Instrum. Methods Phys. Res. A* **382**, 524 (1996).
21. Strüder, L., Lechner, P., and Leutenegger, P., *Naturwissenschaften* **85**, 539 (1998).

22. Kappen, P., Tröger, L., Zink, H., Materlik, G., Reckleben, C., Hansen, K., Grunwaldt, J.-D., and Clausen, B. S., in preparation.
23. Leutenegger, P., Longini, A., Fiorini, C., Struder, L., Kemmer, J., Lechner, P., Sciuti, S., and Cesareo, R., *Nucl. Instrum. Methods Phys. Res. A* **439**, 458 (2000).
24. Hansen, K., and Tröger, L., *IEEE Trans. Nucl. Sci.*, in press.
25. Clausen, B. S., Steffensen, G., Fabius, B., Villadsen, J., Feidenhans'l, R., and Topsøe, H., *J. Catal.* **132**, 524 (1991).
26. Clausen, B. S., Gråbæk, L., Steffensen, G., Hansen, P. L., and Topsøe, H., *Catal. Lett.* **20**, 23 (1993).
27. Clausen, B. S., *Catal. Today* **39**, 293 (1998).
28. Kracht, T., "On-Line: A Program Package for Data Acquisition and Beamline Control at HASYLAB," http://www-hasylab.desy.de/services/computing/on_line/on_line.html., DESY, Hamburg, 2000.
29. Fleet, M. E., *Acta Crystallogr. B* **38**, 1718 (1982).
30. O'Neill, H. S. C., and Dollase, W. A., *Phys. Chem. Miner.* **20**, 541 (1994).
31. Robinson, J. W., "Handbook of Spectroscopy," Vol. I. CRC Press, OH, 1975.
32. Yamashita, H., Matsuoka, M., Tsuji, K., Shioya, Y., Anpo, M., and Che, M., *J. Phys. Chem.* **100**, 397 (1996).
33. Kau, L.-S., Spira-Solomon, J., Penner-Hahn, J. E., Hodgson, K. O., and Solomon, E. I., *J. Am. Chem. Soc.* **109**, 6433 (1987).
34. Clause, O., Bonneviot, L., Che, M., Verdageur, M., Villian, F., Bazin, D., and Dexpert, H., *J. Chim. Phys.* **86**, 1767 (1989).
35. Lamberti, C., Spoto, G., Scarano, D., Pazé, C., Salvalaggio, M., Bordiga, S., Zecchina, A., Palomino, G. T., and D'Acapito, F., *Chem. Phys. Lett.* **269**, 500 (1997).
36. Palomino, G. T., Fisicaro, P., Bordiga, S., Zecchina, A., Giamello, E., and Lambertini, C., *J. Phys. Chem. B.* **104**, 4064 (2000).
37. Kumashiro, R., Kuroda, Y., and Nagao, M., *J. Phys. Chem. B.* **103**, 89 (1999).
38. Grunwaldt, J.-D., Molenbroek, A. M., Topsøe, N.-Y., Topsøe, H., and Clausen, B. S., *J. Catal.* **194**, 452 (2000).
39. Clausen, B. S., Lengeler, B., Rasmussen, B. S., Niemann, W., and Topsøe, H., *J. Phys. (Paris)* **C8**, 237 (1986).
40. Severino, F., Brito, J. L., Laine, J., Fierro, J. L. G., and LopezAgudo, A., *J. Catal.* **177**, 82 (1998).
41. Tonner, S. P., Wainwright, M. S., Trimm, D. L., and Cant, N. W., *Appl. Catal.* **11**, 93 (1984).
42. "Gmelins Handbook of Inorganic Chemistry," Copper, Lfg. 3, part B. Verlag Chemie GmbH, Weinheim/Bergstrasse, 1962.
43. Fubini, B., and Giamello, E., *J. Therm. Anal.* **29**, 655 (1984).
44. Muhler, M., Nielsen, L. P., Törnqvist, E., Clausen, B. S., and Topsøe, H., *Catal. Lett.* **14**, 241 (1992).
45. Matsuoka, M., Takahashi, K., Yamashita, H., and Anpo, M., *J. Phys. IV* **7**, 943 (1997).
46. Liu, D.-J., and Pobota, H. J., *Appl. Catal. B* **4**, 155 (1994).
47. Als-Nielsen, J., Grübel, G., and Clausen, B. S., *Nucl. Instrum. Methods Phys. Res. B* **97**, 522 (1995).
48. Shannon, R., Rogers, D., and Prewitt, C., *Inorg. Chem.* **10**, 719 (1971).